Abnormal Cone Structure in Foveal Schisis Cavities in X-Linked Retinoschisis from Mutations in Exon 6 of the *RS1* Gene

Jacque L. Duncan,[1] Kavitha Ratnam,[1] David G. Birch,[2] Sanna M. Sundquist,[1] Anna S. Lucero,[1] Yuhua Zhang,[3] Meira Meltzer,[4,5] Nizar Smaoui,[6] and Austin Roorda[7]

PURPOSE. To evaluate macular cone structure in patients with X-linked retinoschisis (XLRS) caused by mutations in exon 6 of the *RS1* gene.

METHODS. High-resolution macular images were obtained with adaptive optics scanning laser ophthalmoscopy (AOSLO) and spectral domain optical coherence tomography (SD-OCT) in two patients with XLRS and 27 age-similar healthy subjects. Retinal structure was correlated with best-corrected visual acuity, kinetic and static perimetry, fundus-guided microperimetry, full-field electroretinography (ERG), and multifocal ERG. The six coding exons and the flanking intronic regions of the *RS1* gene were sequenced in each patient.

RESULTS. Two unrelated males, ages 14 and 29, with visual acuity ranging from 20/32 to 20/63, had macular schisis with small relative central scotomas in each eye. The mixed scotopic ERG b-wave was reduced more than the a-wave. SD-OCT showed schisis cavities in the outer and inner nuclear and plexiform layers. Cone spacing was increased within the largest foveal schisis cavities but was normal elsewhere. In each patient, a mutation in exon 6 of the *RS1* gene was identified and was predicted to change the amino acid sequence in the discoidin domain of the retinoschisin protein.

CONCLUSIONS. AOSLO images of two patients with molecularly characterized XLRS revealed increased cone spacing and abnormal packing in the macula of each patient, but cone coverage and function were near normal outside the central foveal schisis cavities. Although cone density is reduced, the preservation of wave-guiding cones at the fovea and eccentric macular regions has prognostic and therapeutic implications for XLRS patients with foveal schisis. (Clinical Trials.gov number, NCT00254605.) (*Invest Ophthalmol Vis Sci.* 2011;52:9614–9623) DOI:10.1167/iovs.11-8600

X-linked juvenile retinoschisis (XLRS) is an inherited retinal degeneration affecting between 1 in 5000 and 1 in 25,000 males.[1–3] The gene responsible for XLRS, *RS1*, is located at Xp22.1 and encodes a soluble 224-amino acid secretory adhesion protein, retinoschisin.[4,5] Retinoschisin comprises an N-terminal signal peptide, the Rs1 domain, a highly conserved discoidin domain important for cell-cell interactions and adhesion, and a short C-terminal segment.[6] Retinoschisin is synthesized and secreted by photoreceptors, forms a disulfide-linked homo-octameric complex,[7–11] and mediates interactions and adhesion between photoreceptor, bipolar, and Müller cells to maintain the structural integrity of the retina.[8,12–14]

XLRS is characterized by splitting, or schisis, affecting all retinal layers. Peripheral schisis cavities are observed in 50% to 70% of XLRS patients,[2,15–17] most commonly inferotemporally.[17] The electroretinogram is a full-field measure of the outer retinal response to light in which a-wave amplitudes are generated by rod and cone photoreceptors and b-wave amplitudes are generated by bipolar cells in response to a bright flash in darkness. The electroretinogram shows a characteristic electronegative pattern in most XLRS patients, with loss of b-wave amplitudes to a greater extent than loss of a-wave amplitudes.[1,18] This finding, along with additional evidence of bipolar cell dysfunction, suggests that XLRS may not affect photoreceptor function directly.[19–21]

Stellate cystic-appearing splitting at the fovea, known as foveal schisis, is present in most patients with XLRS.[15] Foveal schisis may account for reduced central visual acuity,[17] although visual acuity, foveal thickness, and cystic area have not been correlated in other studies.[15] In older patients, retinal pigment epithelial (RPE) atrophy has been observed at the fovea.[15] Although some studies have reported the natural history of XLRS shows little decline in visual acuity over time,[17,22] several studies have reported progressive visual acuity loss over decades, when foveal cysts coalesce to form macrocysts as patients age.[23,24] Foveal atrophy in the fourth to fifth decades of life has been associated with reduced vision, perhaps as an adverse effect of chronic foveal schisis on cone structure.[16] Among 86 patients with *RS1* mutations, visual acuity was reduced with increasing age, and patients older than 30 had significantly more severe macular changes than younger patients,[24] presumably because of chronic disruption of the normal foveal architecture.[16] To determine whether therapies are likely to improve visual prognosis in patients with XLRS, a clearer understanding of the effects that foveal schisis caused by mutations in *RS1* have on cone structure is required.

Definitive histologic studies of cone structure in XLRS have provided limited information not only because of postmortem changes but also because eyes studied histologically have had severe end-stage disease,[25–31] making it difficult to study the effect of *RS1* mutations on foveal cone structure. However, some reports have demonstrated loss of normal cone structure in regions underlying schisis,[29,30] whereas regions of attached retina without schisis showed preserved photoreceptor structure.[25,31] Optical coherence tomography (OCT) has been used to study macular structures in younger, living patients with XLRS and has demonstrated schisis in all retinal layers bridged by vertical palisades,[15,32–38] many in patients with identified *RS1* mutations.[39–41] However, the lateral resolution of commercially available spectral domain OCT (SD-OCT) systems is not sufficient to study the effect of *RS1* mutations on individual cone photoreceptor structure.

It has not been possible to study individual cone photoreceptors affected by XLRS in living patients because optical imperfections in all eyes, healthy or diseased, limit the lateral resolution of retinal images with all the methods commonly used in clinical practice.[42] We and others[43–55] have used adaptive optics to compensate for optical aberrations and significantly improve the resolution of retinal images in patients with inherited retinal degenerations and diseases. In vivo high-resolution studies of macular structure provide a unique opportunity to analyze the structural and functional effects of *RS1* mutations on a cellular level.

In the present study, we characterized the retinal phenotype using adaptive optics scanning laser ophthalmoscopy (AOSLO)[56,57] to obtain single-cell resolution images of macular cones in three eyes of two unrelated patients with mutations in exon 6 of the *RS1* gene, predicted to affect protein structure in the discoidin domain.[24] This noninvasive imaging approach permits correlation between cone structure and function in patients with XLRS caused by mutations in exon 6 of the *RS1* gene.

METHODS

Research procedures were performed in accordance with the Declaration of Helsinki. The study protocol was approved by the University of California at San Francisco and the University of California at Berkeley institutional review boards. Subjects gave written informed consent before participation in any of the studies.

Clinical Examination

A complete history was obtained, including information about all known family members. Measurement of best-corrected visual acuity was performed using a standard eye chart according to the Early Treatment of Diabetic Retinopathy Study protocol. Goldmann kinetic perimetry was performed with V-4e and I-4e targets. Automated static perimetry was completed using a visual field analyzer (Humphrey Visual Field Analyzer II, 750-6116-12.6; Carl Zeiss Meditec, Inc., Dublin, CA) 10–2 SITA-standard threshold protocol with measurement of foveal thresholds, using a Goldmann III stimulus on a white background (31.5 asb) and an exposure duration of 200 ms. Pupils were dilated with 1% tropicamide and 2.5% phenylephrine before color fundus photographs were obtained with fundus autofluorescence (AF) and fluorescein angiograms were obtained using a digital camera (50EX; Topcon, Tokyo, Japan).

Full-field electroretinography (ERG) was performed after 45 minutes of dark adaptation using Burian-Allen contact lens electrodes (Hansen Ophthalmic Development Laboratory, Iowa City, IA), according to International Society for Clinical Electrophysiology and Vision (ISCEV) standards[58] and as described elsewhere.[51] Reduced amplitudes were reported as percentage of mean, and mean values and standard deviations obtained from 200 normal age-similar eyes were used for

comparison. Multifocal ERG testing was performed in a light-adapted state (VERIS 5.2.4X; Electro-Diagnostic Imaging, Inc., Redwood City, CA), using a Burian-Allen contact lens electrode, following ISCEV standards as previously described.[51,59,60] Response densities of the central ring and implicit times were compared with nine healthy controls ranging in age from 14 to 72 years. Fundus-guided microperimetry (MP-1; Nidek Technologies America Inc., Greensboro, NC) tested 45 locations within the central 8° visual field using a Goldmann III stimulus of 200-ms duration with a 4–2 threshold strategy; the subject was asked to fixate on each center of four crosses, each 2° in extent at an eccentricity of 5°. Fixation was monitored with respect to retinal landmarks. Numeric thresholds in decibels (dB) were exported and superimposed on AOSLO images using technical computing software (MatLab; MathWorks, Natick, MA). Mean normal values ± 1 SD across the central 10° for subjects aged 0 to 20 were 19.9 ± 0.4 dB, and for subjects aged 21 to 40 they were 19.5 ± 1.1 dB (Midena E, et al. *IOVS* 2006;47:ARVO E-Abstract 5349).

SD-OCT images were obtained (Spectralis HRA + OCT Laser Scanning Camera System; Heidelberg Engineering, Vista, CA). The infrared beam of the superluminescent diode, with a center wavelength of 870 nm, was used to acquire 20° horizontal scans through the locus of fixation; scans included 100 A-scans/B-scans for images through the locus of fixation and 10 A-scans/B-scans for the 19 horizontal scans used to acquire the 20° × 15° volume scans. Photoreceptor inner segment layer and outer segment layer thickness at the fovea was quantified by manually placing cursors provided with the manufacturer's software at the midpoint of the internal limiting membrane, external limiting membrane, inner segment/outer segment (IS/OS) interface, and OS/RPE interface within 1° of the anatomic fovea to measure outer nuclear layer (ONL), IS, and OS thickness. Optically empty schisis cavities were excluded from the measurements and precluded accurate measurement of the ONL in all but the left eye of patient 1. Five measures separated by 1 pixel were made of each layer along each interface, in each eye, and average thickness measures were compared with measures from seven eyes from age-similar healthy subjects (age range, 23–54 years).

AOSLO Image Acquisition and Cone Spacing Analysis

High-resolution images were obtained using AOSLO in each eye, and images were analyzed using custom-written software to determine cone spacing measures using previously described methods.[51,59] Cone spacing measures were compared with measures from 27 age-similar healthy subjects. Voronoi analysis[61–63] was performed on contiguous patches of unambiguous cones to determine the regularity of the mosaic. The results were compared with results from three age-similar normal eyes at similar eccentricities, cone spacing, or both.

Genetic Testing

Whole blood was obtained for mutation analysis of the *RS1* gene through eyeGENE protocol 06-EI-0236.[4,5] The six coding exons and the flanking intronic regions of the *RS1* gene were amplified by PCR, and the bidirectional sequence was analyzed. The first base of the ATG initiation codon is denoted as nucleotide 1 (RefSeq: NM_000330).

RESULTS

Clinical Characteristics

Two unrelated male patients, aged 14 (patient 1) and 29 (patient 2), were diagnosed with XLRS at ages 8 and 7, respectively, when they had trouble seeing the blackboard at school. Both patients reported reduced night vision since early childhood. Patient 1 was of Native American (Choctaw and Cheyenne River Sioux) descent while patient 2 was from Mexico. Patient 1 had a 7-year-old brother and two older sisters with normal eye examination results; patient 2 had one older brother with vision loss who lived in Mexico and was not

available for examination; there was no other family history of vision loss or consanguinity in either family. Clinical characteristics of the patients are presented in Table 1. See Supplementary Table S1 (http://www.iovs.org/lookup/suppl/doi:10.1167/iovs.11-8600/-/DCSupplemental) for full-field ERG and multifocal ERG data. Both patients showed relative central scotomas with reduced foveal sensitivities in each eye. Stellate macular schisis and preretinal vitreous veils were present in each eye of each patient, although the fovea was minimally affected in the left eye of patient 1 (Fig. 1, top panels). AF was relatively homogeneous in the macula of each eye of patient 1, despite large schisis cavities in the right eye. In patient 2, however, AF was increased in the large foveal schisis cavities with stellate linear regions of reduced AF corresponding to foveal schisis cavity walls in each macula (Fig. 1, middle panels).

Retinal Thickness

OCT showed large central foveal cyst-like spaces surrounded by schisis in the inner nuclear layer (INL) and ONL with vertical palisades in the right eye of patient 1 and in both eyes of patient 2 (Fig. 1, bottom panels); in patient 1, there were no foveal cysts in the left eye. In patient 1, the walls of multiple small schisis cavities precluded acquisition of clear images of cone mosaics using AOSLO within the schisis cavities in the right eye (Fig. 1, left bottom) and in regions greater than 2° eccentric to the fovea in the left eye. In patient 2, large central cysts permitted imaging of cone mosaics using AOSLO within the schisis cavities in both eyes. In each eye of patient 2, many small schisis cavities were observed in the INL and ONL in and around the fovea. In each patient, laminar structure (corresponding to the external limiting membrane, IS/OS interface, posterior tips of OS, and RPE cells) was abnormal throughout the macula. The IS/OS interface was variable in thickness and reflectivity throughout the fovea, and the increase in photoreceptor length at the fovea seen in healthy subjects was absent. Foveal schisis precluded accurate measurement of ONL thickness in all but the left eye of patient 1, in whom the ONL was significantly thinner than normal ($P = 4.5 \times 10^{-13}$; Table 1). Schisis cavities were present in the IS layer of the right eye of patient 1, but in all other eyes the IS were significantly thinner than normal ($P < 3.5 \times 10^{-5}$; Table 1). OS were significantly shorter than normal in each patient ($P < 0.02$) (Fig. 1, bottom, Table 1).

Retinal images were obtained using AOSLO and revealed schisis walls with high resolution (patient 1, Fig. 2A; patient 2 right eye, Fig. 3A; patient 2 left eye, Fig. 4A). Anatomic foveola was estimated by retinal landmarks. The preferred retinal locus (PRL) was identified by using a fixation stimulus integrated into the raster scan of the AOSLO.[64] Walls of tiny schisis cavities prevented imaging of unambiguous cone mosaics beyond the central 2° in the left eye of patient 1. Regions of increased cone spacing were identified within 2° of the fovea in each eye imaged. However, in patient 2, in whom cones were visualized at eccentricities greater than 2°, cone spacing was normal (Figs. 3C, 4C, 5). With a few exceptions, increased cone spacing correlated with reduced sensitivities measured with fundus-guided microperimetry in each eye imaged with AOSLO (Figs. 2B, 2C, 3B, 3C, 4B, 4C).

Regions encompassing contiguous and unambiguous cones (range, 78–121 cones per set) were selected for Voronoi testing. For patient 2, all contiguous regions were from the right eye and were inside the limits of the large foveal schisis cavity. Schisis walls disrupted the contiguity of cones and precluded analysis of cone packing in regions outside the largest central schisis cavity in the right eye and throughout the image in the left eye. Results of the analysis are shown in Supplemen-

TABLE 1. Clinical Characteristics of Patients

Patient	Age (y)	Genotype	Eye	BCVA	ETDRS Score	Foveal Threshold (dB)	Kinetic Perimetry	SD-OCT Foveal ONL Thickness (μm)	SD-OCT Foveal IS Thickness (μm)	SD-OCT Foveal OS Thickness (μm)
1	14	c.626G>C, p.Arg209Pro	OD	20/50	65	34	Constriction to 40° nasally OD, 50° OS to V4e target	Schisis	Schisis	29.8 ± 0.8 ($P = 4 \times 10^{-7}$)
			OS	20/32−2	73	36		65.2 ± 0.8 ($P = 4.7 \times 10^{-13}$)	26.0 ± 1.2 ($P = 4 \times 10^{-5}$)	38.2 ± 0.8 ($P = 0.02$)
2	29	c.579dupC; p. Ile194Hisfs	OD	20/50−1	64	34	Full to V4e and I4e OD, constricted to 40° nasally to V4e target	Schisis	24.6 ± 1.1 ($P = 2 \times 10^{-6}$)	21.2 ± 0.8 ($P = 5 \times 10^{-12}$)
			OS	20/63	60	34	OS	Schisis	23.0 ± 0.7 ($P = 4 \times 10^{-8}$)	21.2 ± 0.4 ($P = 5 \times 10^{-12}$)

Foveal thresholds were measured using the Humphrey visual field 10–2 SITA standard protocol. SD-OCT thickness values represent the average of five measures within 1° of the fovea. Mean normal foveal ONL thickness = 125.5 ± 13.1 μm. Mean normal foveal IS thickness = 32.6 ± 3.2 μm. Mean normal foveal OS thickness = 43.7 ± 5.3 μm. BCVA, best-corrected visual acuity; ETDRS, Early Treatment Diabetic Retinopathy Study visual acuity score, expressed as number of letters correctly identified.
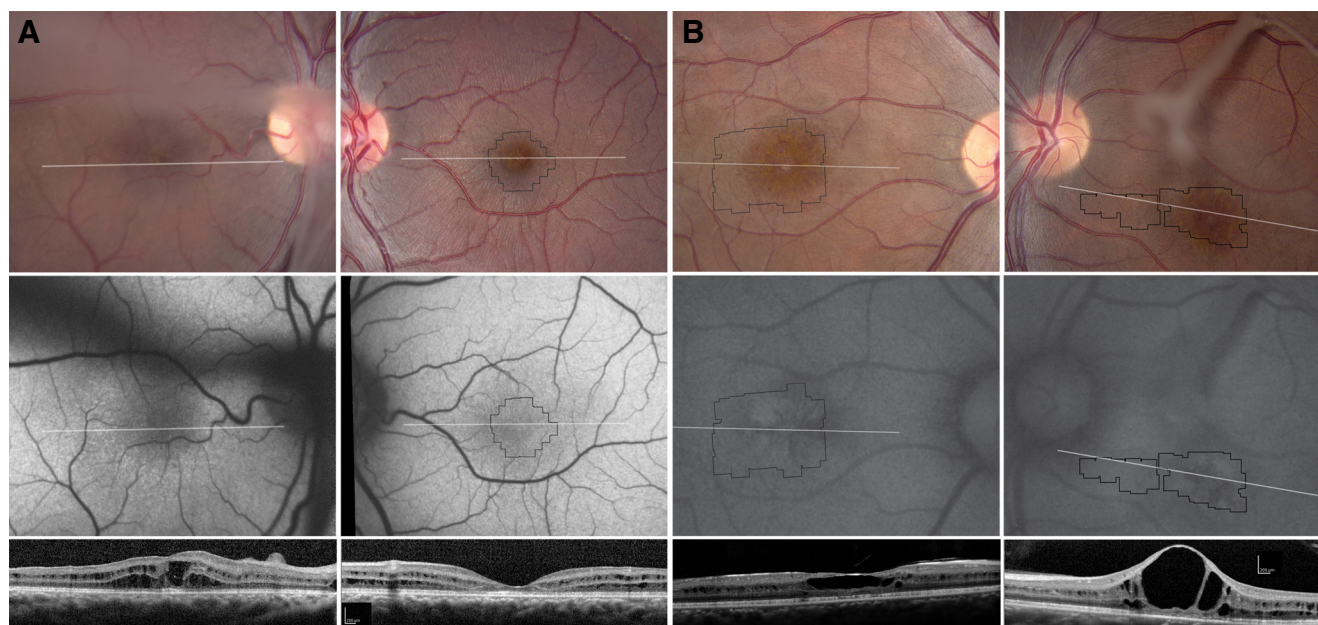
FIGURE 1. Color (*top*), AF (*middle*), and SD-OCT images (*bottom*) of the right (*left column*) and left (*right column*) eyes of XLRS patient 1 (**A**) and patient 2 (**B**). Locations of the AOSLO images (Figures 2–4) are indicated by the *thin, black outlines*. SD-OCT locations are shown by the *horizontal white lines*. Vitreous veils created dark shadows visible in AF images of the right eye of patient 1 and the left eye of patient 2 and precluded acquisition of AOSLO images in the right eye of patient 1.

tary Table S2 (http://www.iovs.org/lookup/suppl/doi:10.1167/iovs.11-8600/-/DCSupplemental). In addition to being less dense, all metrics demonstrated that the cones in the XLRS patient were also less regular within the central foveal schisis cavity. Supplementary Fig. S1 (http://www.iovs.org/lookup/suppl/doi:10.1167/iovs.11-8600/-/DCSupplemental), which shows the Voronoi domains superimposed on the AOSLO image, illustrates the difference in packing between healthy and XLRS patients.

Genetic Test Results

The *RS1* gene in patient 1 contained a hemizygous G→C change at nucleotide 626 in exon 6, changing the amino acid arginine (Arg) to proline (Pro) in the discoidin domain of the retinoschisin protein. Although this variation has not been previously reported in the literature, mutations at the same codon leading to different amino acid substitutions (p.Arg209His, p.Arg209Cys, p.Arg209Gly, p.Arg209leu) have been reported in patients with XLRS[4,5,65–68] (http://www.dmd.nl/rs.html). In patient 2, the *RS1* gene contained a hemizygous C duplication at nucleotide 579 in exon 6 (c.579dupC), reported previously in XLRS patients.[5,24,69,70] This mutation changes the amino acid isoleucine (Ile) to histidine (His) at residue 194 and creates a frameshift in the retinoschisin protein (p.Ile194Hisfs).[5] The mutation is predicted to disrupt the discoidin domain and to result in premature truncation[5,24] (http://www.dmd.nl/rs.html).

DISCUSSION

In the present study, we addressed a major challenge that limits understanding of the effects of *RS1* mutations on photoreceptor structure, namely the inability to study single cells in living eyes. We used AOSLO to obtain single-cell resolution images of the macular cones in two patients with mutations in the discoidin domain of the retinoschisin protein. Our findings are summarized in Table 2.

Patient 1, who had no foveal schisis in the left eye, used the anatomic fovea for fixation. Visual acuity was lower than normal (20/32), likely because of a combination of reduced sensitivity and increased cone spacing at that location. In patient 2, similar increases in cone spacing were observed in the fovea, but foveal schisis appears to have affected the synaptic connections between the photoreceptors and the inner retina, leading to more profound sensitivity loss. As a result, patient 2 uses an eccentric fixation location, choosing a retinal region with relatively preserved cone spacing (right eye: fixation ~1° temporal, cone spacing z-score = −0.6; left eye: fixation ~2° nasal, cone spacing z-score = 1.2). Despite the normal spacing, acuity is lower than expected for normal eyes at those eccentricities; visual acuity is expected to be 20/30 at 1° and better than 20/40 at 2°.[71] In the present study, fundus-guided microperimetry showed central scotomas with 1 to 2 log units of sensitivity loss in regions with increased cone spacing (z-score range, 2.4–5.7). However, the correlation between microperimetry scores and cone spacing z-scores showed several regions in which cone spacing was not correlated with sensitivity; either cone spacing was near normal with reduced sensitivity or cone spacing was abnormal in a region with relatively preserved sensitivity. This discrepancy may be due to dysfunction of synaptic connections caused by schisis. However, fundus-guided microperimetry scores were made using a system in which fundus landmarks are tracked using a low-resolution infrared fundus image; the resolution of these measures is not commensurate with the single-cell resolution recorded using AOSLO. More precise comparisons between retinal sensitivity and cone spacing abnormalities would require the delivery of visual stimuli through modulation of the AOSLO scanning laser used to image the retina (Tuten WS, et al. *IOVS* 2011;52:ARVO E-Abstract 4459).

The present study supports a correlation between the degree of abnormality in macular structure and function based on SD-OCT, fundus-guided microperimetry, and AOSLO that might not have been evident in previous studies
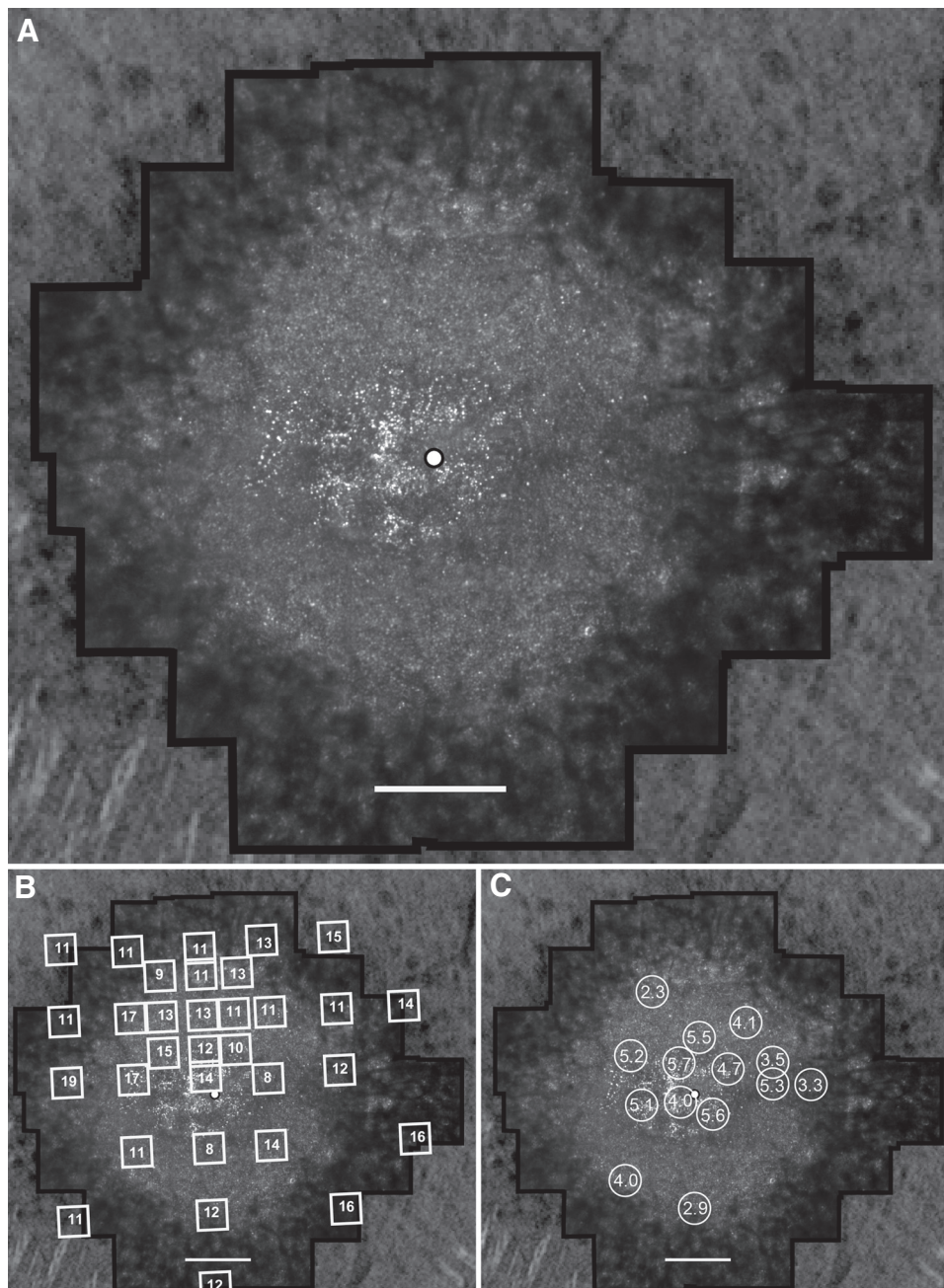
FIGURE 2. **(A)** AOSLO image of the left eye of patient 1. **(B)** Fundus-guided microperimetry scores superimposed on AOSLO image. **(C)** Cone spacing z-scores superimposed on AOSLO image. Sensitivities are reduced by 1 to 2 log units, and cone spacing is increased by 2.3 to 5.7 SD from normal. The *white circle* with a *black outline* indicates the preferred locus for fixation, which coincides with the anatomic fovea. Scale bar, 1° (~300 μm).

using lower resolution imaging techniques. Changes in cone spacing and packing within the foveal schisis cavities suggest that chronic disruption of foveal architecture results in cone loss in XLRS but that many cones are preserved and act as effective optical waveguides. Eccentric to large central schisis cavities, the cones are well preserved, despite diffusely abnormal macular structures identified on SD-OCT. This observation suggests therapeutic interventions designed to normalize foveal structure, such as carbonic anhydrase inhibitors, and treatment to replace normal retinoschisin may be likely to improve visual function and cone survival in patients with XLRS.

We observed focally increased AF and increased cone spacing within large foveal schisis cavities in patient 2, as others have reported in patients with XLRS[67,70,72,73] and isolated foveal retinoschisis.[74] The radial hyperautofluorescence of the central macula corresponding to schisis cavities

may be caused by differences in retinal thickness, shadowing effects of schisis cavity walls, effects of alterations in macular pigment content, or changes in the RPE lipofuscin content,[72] perhaps representing an increase in photoreceptor-RPE metabolic load before cell loss and atrophy.[70] AF changes in XLRS may not be caused by RPE dysfunction, as in other forms of retinal degeneration, but instead may indicate the variability of retinal light transmission caused by schisis walls, disruption of macular pigment, or fluorophores in schisis cavity fluid.[67] In conjunction with the increased cone spacing we observed within the schisis cavities, the increased AF may indicate RPE cells are present but abnormal, in response to chronic disruption of the overlying retina and cone loss.

Several possible explanations, alone or in combination, may account for the increased cone spacing we observed near the anatomic fovea in the XLRS patients we studied.
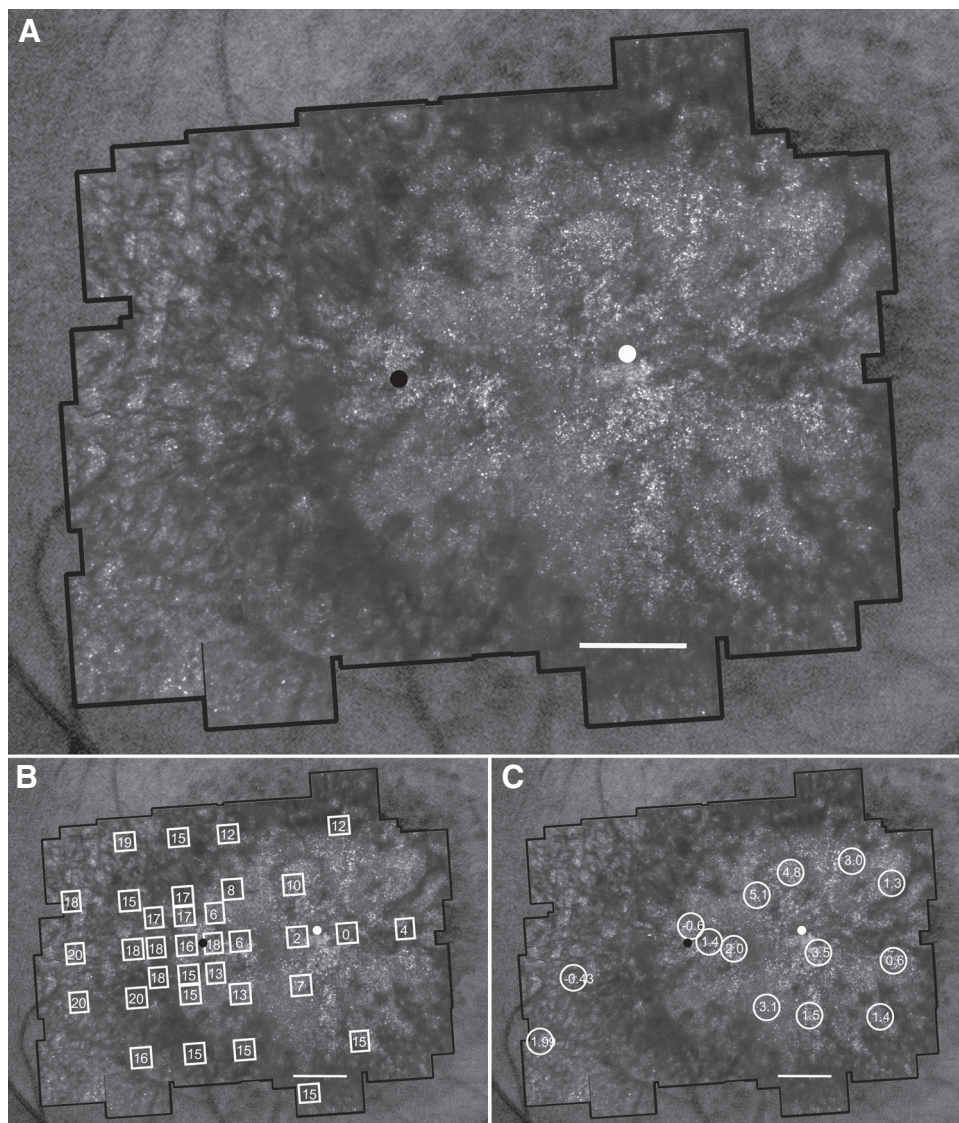
FIGURE 3. (**A**) AOSLO image of the right eye of patient 2. (**B**) Fundus-guided microperimetry scores superimposed on AOSLO image. (**C**) Cone spacing z-scores superimposed on AOSLO image. Sensitivities and cone spacing are near normal temporal-to-large central foveal schisis cavities seen on SD-OCT. The *white circle* indicates the anatomic fovea, and the *black circle* indicates the PRL. Scale bar, 1° (~300 μm).

Intracellular Retention of Mutant Retinoschisin Results in Increased Cone Size

It is possible that abnormal mutant retinoschisin accumulates within swollen, abnormal cone IS and causes increased cone spacing. However, all photoreceptors in these hemizygous male patients express mutant retinoschisin, which would most likely be retained within all photoreceptors throughout the retina. Given that we observed increased cone spacing focally near the fovea with regions of normal cone spacing, this explanation is less likely.

Intraretinal Fluid Alters the Retinal Refractive Index and Results in Apparent Increases in Cone Spacing

A magnification artifact generated from a "fluid lens" within the central foveal schisis cavities could give rise to apparent increases in cone spacing. However, this possibility is unlikely because the refractive index changes are expected to be very small and the photoreceptors are very close to the posterior side of the cavities (objects held close to a lens will not appear magnified). In addition, cone spacing near the anatomic fovea was equally, if not more, abnormal in patient

1, who showed no foveal schisis, as in patient 2, who showed large foveal schisis.

The Fovea Develops Abnormally in the Absence of Normal Retinoschisin

If retinoschisin is required for normal foveal development, the absence of normal retinoschisin may produce a fovea with increased cone spacing or reduced cone density, which may be stable over time. Retinoschisin is required for normal development and maintenance of retinal structure.[14,31,75] During development, there is massive migration of the cone photoreceptors inward and of inner retinal neurons outward.[76-78] This migration forces the foveal retinal cells to make connections radially, creating Henle's fiber layer, rather than vertically, as elsewhere in the retina. A mechanism by which cellular displacement creates the foveal pit may involve interactions between cones and Müller cells at the outer limiting membrane. As Müller cells are stretched laterally when the foveal pit forms, these stretching forces squeeze the cones together to create the foveal pit.[76,79] In the absence of retinoschisin, interactions between Müller cells and cones are likely compromised, not only predisposing to the formation of schisis cavities but perhaps also preventing normal foveal development. Longitudinal
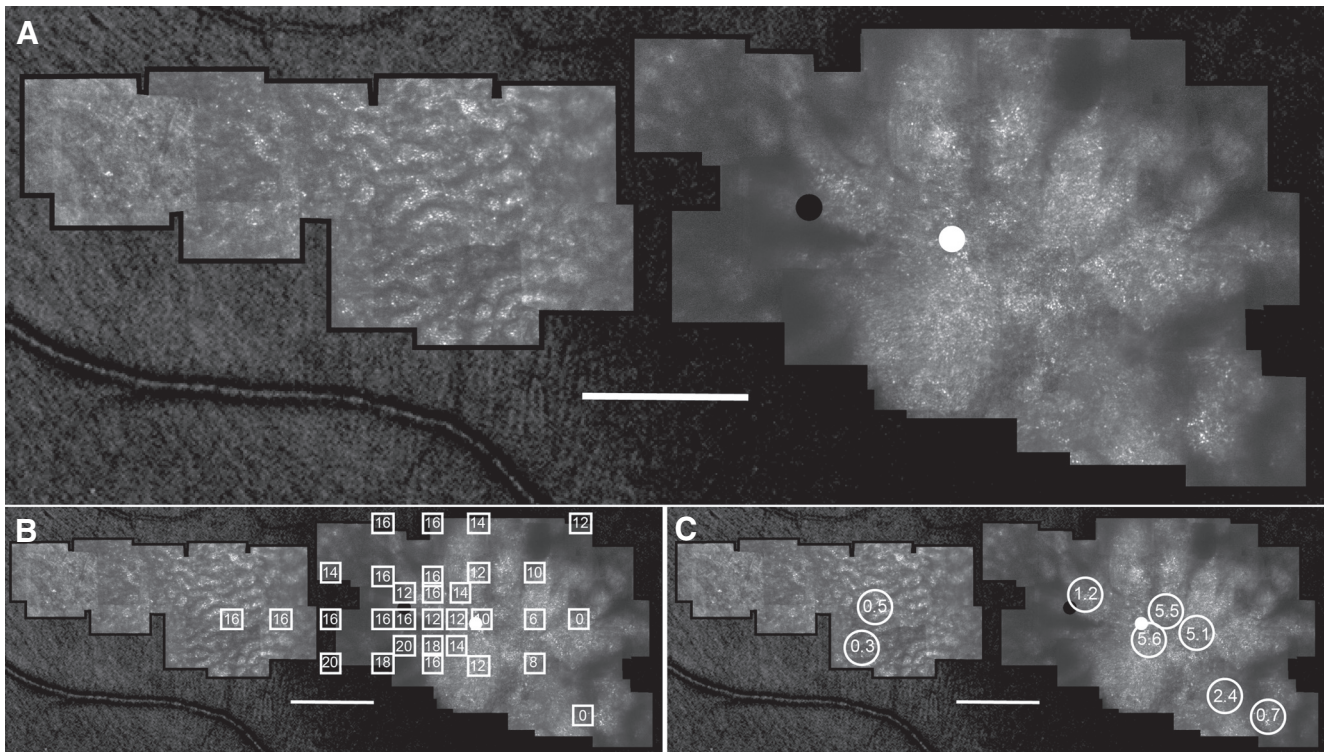
FIGURE 4. (**A**) AOSLO image of the left eye of patient 2. (**B**) Fundus-guided microperimetry scores superimposed on AOSLO image. (**C**) Cone spacing z-scores superimposed on AOSLO image. Sensitivities and cone spacing are near normal nasal-to-large central foveal schisis cavities seen on SD-OCT. The *white circle* indicates the anatomic fovea, and the *black circle* indicates the PRL. Scale bar, 1° (~300 μm).

studies of XLRS patients with AOSLO showing stable cone spacing over time would support this hypothesis. If the increased foveal cone spacing we observed results from a non-progressive developmental abnormality, therapies to improve retinal structure with the administration of normal retinoschi-sin may be of great benefit, especially if administered early in life.

Chronic Disruption of Normal Foveal Structure Causes Photoreceptor Loss

It is possible that intraretinal fluid or disruption of connections between photoreceptors and inner retinal cells causes photo-

FIGURE 5. Cone spacing in the maculae of three eyes with XLRS. In patient 1, walls of small schisis cavities precluded measurement of cone spacing beyond 2° eccentricity. Cone spacing was increased within the central 2° but was normal at greater eccentricities imaged in patient 2.

receptor degeneration over time. Cone spacing was within normal limits in regions affected by diffuse schisis, with smaller cavities in patient 2. In contrast, patients with photoreceptor degeneration caused by mutations in retinitis pigmentosa GTPase regulator (RPGR),[51] rhodopsin,[80] or mitochondrial DNA[63] show increased cone spacing diffusely throughout the macula. Our results suggest that the *RS1* mutation in patient 2 did not cause diffuse degeneration of cones throughout the macula but that regions of increased cone spacing and reduced visual function were limited to the central foveal schisis cavi-ties in which retinal structure was most disrupted, perhaps indicating that cone degeneration occurs secondary to disrup-tion of the inner retinal layers. Although there are no histologic studies of foveal cones that lie beneath schisis cavities in XLRS patients, studies of cystoid macular edema show intraretinal fluid accumulation that causes cell displacement and splitting of the perifoveal retina within the same layers affected in XLRS.[81-83] Cystoid macular edema is believed to cause re-duced acuity by compression of retinal neurons, nerve fibers, and capillaries, with photoreceptor degeneration over time.[84] A similar mechanism may cause cone loss in XLRS patients. This hypothesis predicts that therapies, such as carbonic an-hydrase inhibitors, designed to improve retinal structure by reducing schisis volume would result in improved foveal cone function and survival over time.[85-88]

In addition, if the degeneration of cone photoreceptors is limited to regions near the anatomic fovea affected by large schisis cavities, therapies for XLRS may be more likely to succeed than therapies for retinal degenerations that cause photoreceptor degeneration diffusely and directly. Although synaptic abnormalities were present in the outer plexiform layer in mice deficient in *Rs1h*, the mouse ortholog of the human *RS1* gene,[89] the ONL contained a normal number of photoreceptor nuclei at 1 month, with slowly progressive loss of nuclei beginning from 1 month to 4 months of age

TABLE 2. Summary of Findings

Patient	Cone Spacing in Large Central Schisis Cavities	Cone Spacing Eccentric to Schisis Cavities	Preferred Retinal Locus of Fixation	Macular SD-OCT	Foveal AF Abnormalities
1	Increased with irregular packing structure	Not imaged	Fovea	Diffuse macular schisis; no central cavity OS; reduced ONL, IS, and OS thicknesses	Decreased foveal AF; radial reduced AF associated with schisis walls
2	Increased with irregular packing structure	Normal	1° to 2° eccentric to the fovea in regions with preserved cone spacing	Diffuse macular schisis; large central cavities OU; reduced ONL, IS, and OS thicknesses	Focally increased foveal AF; radial reduced AF associated with schisis walls

and continuing through 16 months of age.[90] Adeno-associated viral vector-delivered human *RS1* resulted in substantial recovery of retinal structure and visual function in *Rs1h*-deficient mice.[6,89–92] When expressed in the same cells as disease-causing mutant retinoschisin, wild-type retinoschisin was folded, assembled into octamers, and secreted in nearly all disease-causing mutants studied.[93] These findings suggest XLRS may be a suitable candidate for therapeutic trials because gene or protein replacement therapy might result in wild-type retinoschisin secretion and improved retinal structure and function in patients independent of the causative mutation. AOSLO may provide a sensitive measure of disease progression in regions with increased cone spacing when correlated with high-resolution measures of retinal thickness and visual function.

References

1. George ND, Yates JR, Moore AT. X linked retinoschisis. *Br J Ophthalmol.* 1995;79:697–702.
2. Sieving PA. Juvenile retinoschisis. In: Traboulsi EI, ed. *Genetic Diseases of the Eye.* New York: Oxford University Press; 1998: 347–355.
3. Tantri A, Vrabec TR, Cu-Unjieng A, Frost A, Annesley WH Jr, Donoso LA. X-linked retinoschisis: a clinical and molecular genetic review. *Surv Ophthalmol.* 2004;49:214–230.
4. Sauer CG, Gehrig A, Warneke-Wittstock R, et al. Positional cloning of the gene associated with X-linked juvenile retinoschisis. *Nat Genet.* 1997;17:164–170.
5. Functional implications of the spectrum of mutations found in 234 cases with X-linked juvenile retinoschisis: the Retinoschisis Consortium. *Hum Mol Genet.* 1998;7:1185–1192.
6. Molday LL, Min SH, Seeliger MW, et al. Disease mechanisms and gene therapy in a mouse model for X-linked retinoschisis. *Adv Exp Med Biol.* 2006;572:283–289.
7. Molday LL, Hicks D, Sauer CG, Weber BH, Molday RS. Expression of X-linked retinoschisis protein RS1 in photoreceptor and bipolar cells. *Invest Ophthalmol Vis Sci.* 2001;42:816–825.
8. Reid SN, Akhmedov NB, Piriev NI, Kozak CA, Danciger M, Farber DB. The mouse X-linked juvenile retinoschisis cDNA: expression in photoreceptors. *Gene.* 1999;227:257–266.
9. Wang T, Zhou A, Waters CT, O'Connor E, Read RJ, Trump D. Molecular pathology of X linked retinoschisis: mutations interfere with retinoschisin secretion and oligomerisation. *Br J Ophthalmol.* 2006;90:81–86.
10. Wu WW, Molday RS. Defective discoidin domain structure, subunit assembly, and endoplasmic reticulum processing of retinoschisin are primary mechanisms responsible for X-linked retinoschisis. *J Biol Chem.* 2003;278:28139–28146.
11. Wu WW, Wong JP, Kast J, Molday RS. RS1, a discoidin domain-containing retinal cell adhesion protein associated with X-linked retinoschisis, exists as a novel disulfide-linked octamer. *J Biol Chem.* 2005;280:10721–10730.
12. Grayson C, Reid SN, Ellis JA, et al. Retinoschisin, the X-linked retinoschisis protein, is a secreted photoreceptor protein, and is expressed and released by Weri-Rb1 cells. *Hum Mol Genet.* 2000; 9:1873–1879.
13. Molday LL, Wu WW, Molday RS. Retinoschisin (RS1), the protein encoded by the X-linked retinoschisis gene, is anchored to the surface of retinal photoreceptor and bipolar cells through its interactions with a Na/K ATPase-SARM1 complex. *J Biol Chem.* 2007;282:32792–32801.
14. Reid SN, Yamashita C, Farber DB. Retinoschisin, a photoreceptor-secreted protein, and its interaction with bipolar and Mueller cells. *J Neurosci.* 2003;23:6030–6040.
15. Apushkin MA, Fishman GA, Janowicz MJ. Correlation of optical coherence tomography findings with visual acuity and macular lesions in patients with X-linked retinoschisis. *Ophthalmology.* 2005;112:495–501.
16. George ND, Yates JR, Moore AT. Clinical features in affected males with X-linked retinoschisis. *Arch Ophthalmol.* 1996;114:274–280.
17. Kellner U, Brummer S, Foerster MH, Wessing A. X-linked congenital retinoschisis. *Graefes Arch Clin Exp Ophthalmol.* 1990;228: 432–437.
18. Peachey NS, Fishman GA, Derlacki DJ, Brigell MG. Psychophysical and electroretinographic findings in X-linked juvenile retinoschisis. *Arch Ophthalmol.* 1987;105:513–516.
19. Alexander KR, Fishman GA, Grover S. Temporal frequency deficits in the electroretinogram of the cone system in X-linked retinoschisis. *Vision Res.* 2000;40:2861–2868.
20. Khan NW, Jamison JA, Kemp JA, Sieving PA. Analysis of photoreceptor function and inner retinal activity in juvenile X-linked retinoschisis. *Vision Res.* 2001;41:3931–3942.
21. Shinoda K, Ohde H, Mashima Y, et al. On- and off-responses of the photopic electroretinograms in X-linked juvenile retinoschisis. *Am J Ophthalmol.* 2001;131:489–494.
22. Apushkin MA, Fishman GA, Rajagopalan AS. Fundus findings and longitudinal study of visual acuity loss in patients with X-linked retinoschisis. *Retina.* 2005;25:612–618.
23. Harris GS, Yeung J. Maculopathy of sex-linked juvenile retinoschisis. *Can J Ophthalmol.* 1976;11:1–10.
24. Pimenides D, George ND, Yates JR, et al. X-linked retinoschisis: clinical phenotype and RS1 genotype in 86 UK patients. *J Med Genet.* 2005;42:e35.
25. Yanoff M, Kertesz Rahn E, Zimmerman LE. Histopathology of juvenile retinoschisis. *Arch Ophthalmol.* 1968;79:49–53.
26. Manschot WA. Pathology of hereditary juvenile retinoschisis. *Arch Ophthalmol.* 1972;88:131–138.
27. Condon GP, Brownstein S, Wang NS, Kearns JA, Ewing CC. Congenital hereditary (juvenile X-linked) retinoschisis: histopathologic and ultrastructural findings in three eyes. *Arch Ophthalmol.* 1986; 104:576–583.
28. Laatikainen L, Tarkkanen A, Saksela T. Hereditary X-linked retinoschisis and bilateral congenital retinal detachment. *Retina.* 1987;7: 24–27.
29. Kirsch LS, Brownstein S, de Wolff-Rouendaal D. A histopathological, ultrastructural and immunohistochemical study of congenital hereditary retinoschisis. *Can J Ophthalmol.* 1996;31:301–310.
30. Ando A, Takahashi K, Sho K, Matsushima M, Okamura A, Uyama M. Histopathological findings of X-linked retinoschisis with neovascular glaucoma. *Graefes Arch Clin Exp Ophthalmol.* 2000;238:1–7.
31. Mooy CM, Van Den Born LI, Baarsma S, et al. Hereditary X-linked juvenile retinoschisis: a review of the role of Mueller cells. *Arch Ophthalmol.* 2002;120:979–984.

32. Azzolini C, Pierro L, Codenotti M, Brancato R. OCT images and surgery of juvenile macular retinoschisis. *Eur J Ophthalmol.* 1997; 7:196–200.

33. Brucker AJ, Spaide RF, Gross N, Klancnik J, Noble K. Optical coherence tomography of X-linked retinoschisis. *Retina.* 2004;24: 151–152.

34. Minami Y, Ishiko S, Takai Y, et al. Retinal changes in juvenile X linked retinoschisis using three dimensional optical coherence tomography. *Br J Ophthalmol.* 2005;89:1663–1664.

35. Ozdemir H, Karacorlu S, Karacorlu M. Optical coherence tomography findings in familial foveal retinoschisis. *Am J Ophthalmol.* 2004;137:179–181.

36. Stanga PE, Chong NH, Reck AC, Hardcastle AJ, Holder GE. Optical coherence tomography and electrophysiology in X-linked juvenile retinoschisis associated with a novel mutation in the XLRS1 gene. *Retina.* 2001;21:78–80.

37. Prenner JL, Capone A Jr, Ciaccia S, Takada Y, Sieving PA, Trese MT. Congenital X-linked retinoschisis classification system. *Retina.* 2006;26:S61–S64.

38. Urrets-Zavalia JA, Venturino JP, Mercado J, Urrets-Zavalia EA. Macular and extramacular optical coherence tomography findings in X-linked retinoschisis. *Ophthalmic Surg Lasers Imaging.* 2007;38: 417–422.

39. Chan WM, Choy KW, Wang J, et al. Two cases of X-linked juvenile retinoschisis with different optical coherence tomography findings and RS1 gene mutations. *Clin Exp Ophthalmol.* 2004;32:429–432.

40. Eriksson U, Larsson E, Holmstrom G. Optical coherence tomography in the diagnosis of juvenile X-linked retinoschisis. *Acta Ophthalmol Scand.* 2004;82:218–223.

41. Gerth C, Zawadzki RJ, Werner JS, Heon E. Retinal morphological changes of patients with X-linked retinoschisis evaluated by Fourier-domain optical coherence tomography. *Arch Ophthalmol.* 2008;126:807–811.

42. Liang J, Williams DR. Aberrations and retinal image quality of the normal human eye. *J Opt Soc Am A Opt Image Sci Vis.* 1997;14: 2873–2883.

43. Liang J, Williams DR, Miller DT. Supernormal vision and high-resolution retinal imaging through adaptive optics. *J Opt Soc Am A Opt Image Sci Vis.* 1997;14:2884–2892.

44. Roorda A, Williams DR. The arrangement of the three cone classes in the living human eye. *Nature.* 1999;397:520–522.

45. Brainard DH, Roorda A, Yamauchi Y, et al. Functional consequences of the relative numbers of L and M cones. *J Opt Soc Am A Opt Image Sci Vis.* 2000;17:607–614.

46. Carroll J, Neitz M, Hofer H, Neitz J, Williams DR. Functional photoreceptor loss revealed with adaptive optics: an alternate cause of color blindness. *Proc Natl Acad Sci USA.* 2004;101:8461–8466.

47. Neitz J, Carroll J, Yamauchi Y, Neitz M, Williams DR. Color perception is mediated by a plastic neural mechanism that is adjustable in adults. *Neuron.* 2002;35:783–792.

48. Pallikaris A, Williams DR, Hofer H. The reflectance of single cones in the living human eye. *Invest Ophthalmol Vis Sci.* 2003;44: 4580–4592.

49. Roorda A, Metha AB, Lennie P, Williams DR. Packing arrangement of the three cone classes in primate retina. *Vision Res.* 2001;41: 1291–1306.

50. Roorda A, Williams DR. Optical fiber properties of individual human cones. *J Vision.* 2002;2:404–412.

51. Duncan JL, Zhang Y, Gandhi J, et al. High-resolution imaging with adaptive optics in patients with inherited retinal degeneration. *Invest Ophthalmol Vis Sci.* 2007;48:3283–3291.

52. Chen Y, Ratnam K, Sundquist SM, et al. Cone photoreceptor abnormalities correlate with vision loss in patients with Stargardt disease. *Invest Ophthalmol Vis Sci.* 2011;52:3281–3292.

53. Choi SS, Doble N, Hardy JL, et al. In vivo imaging of the photoreceptor mosaic in retinal dystrophies and correlations with visual function. *Invest Ophthalmol Vis Sci.* 2006;47:2080–2092.

54. Michaelides M, Rha J, Dees EW, et al. Integrity of the cone photoreceptor mosaic in oligocone trichromacy. *Invest Ophthalmol Vis Sci.* 2011;52:4757–4764.

55. Ooto S, Hangai M, Takayama K, et al. High-resolution photoreceptor imaging in idiopathic macular telangiectasia type 2 using adaptive optics scanning laser ophthalmoscopy. *Invest Ophthalmol Vis Sci.* 2011;52:5541–5550.

56. Roorda A, Romero-Borja F, Donnelly W III, Queener H, Hebert T, Campbell MCW. Adaptive optics scanning laser ophthalmoscopy. *Opt Express.* 2002;10:405–412.

57. Zhang Y, Roorda A. Evaluating the lateral resolution of the adaptive optics scanning laser ophthalmoscope. *J Biomed Opt.* 2006;11: 014002.

58. Marmor MF, Holder GE, Seeliger MW, Yamamoto S. Standard for clinical electroretinography (2004 update). *Doc Ophthalmol.* 2004;108:107–114.

59. Roorda A, Zhang Y, Duncan JL. High-resolution in vivo imaging of the RPE mosaic in eyes with retinal disease. *Invest Ophthalmol Vis Sci.* 2007;48:2297–2303.

60. Duncan JL, Talcott KE, Ratnam K, et al. Cone structure in retinal degeneration associated with mutations in the peripherin/RDS gene. *Invest Ophthalmol Vis Sci.* 2011;52:1557–1566.

61. Baraas RC, Carroll J, Gunther KL, et al. Adaptive optics retinal imaging reveals S-cone dystrophy in tritan color-vision deficiency. *J Opt Soc Am A Opt Image Sci Vis.* 2007;24:1438–1447.

62. Li KY, Roorda A. Automated identification of cone photoreceptors in adaptive optics retinal images. *J Opt Soc Am A Opt Image Sci Vis.* 2007;24:1358–1363.

63. Yoon MK, Roorda A, Zhang Y, et al. Adaptive optics scanning laser ophthalmoscopy images in a family with the mitochondrial DNA T8993C mutation. *Invest Ophthalmol Vis Sci.* 2009;50:1838–1847.

64. Poonja S, Patel S, Henry L, Roorda A. Dynamic visual stimulus presentation in an adaptive optics scanning laser ophthalmoscope. *J Refract Surg.* 2005;21:S575–S580.

65. Li X, Ma X, Tao Y. Clinical features of X linked juvenile retinoschisis in Chinese families associated with novel mutations in the RS1 gene. *Mol Vis.* 2007;13:804–812.

66. Ma X, Li X, Wang L. Novel XLRS1 gene mutations cause X-linked juvenile retinoschisis in Chinese families. *Jpn J Ophthalmol.* 2008; 52:48–51.

67. Renner AB, Kellner U, Fiebig B, Cropp E, Foerster MH, Weber BH. ERG variability in X-linked congenital retinoschisis patients with mutations in the RS1 gene and the diagnostic importance of fundus autofluorescence and OCT. *Doc Ophthalmol.* 2008;116:97–109.

68. Riveiro-Alvarez R, Trujillo-Tiebas MJ, Gimenez-Pardo A, et al. Correlation of genetic and clinical findings in Spanish patients with X-linked juvenile retinoschisis. *Invest Ophthalmol Vis Sci.* 2009; 50:4342–4350.

69. Gehrig A, White K, Lorenz B, Andrassi M, Clemens S, Weber BH. Assessment of RS1 in X-linked juvenile retinoschisis and sporadic senile retinoschisis. *Clin Genet.* 1999;55:461–465.

70. Tsang SH, Vaclavik V, Bird AC, Robson AG, Holder GE. Novel phenotypic and genotypic findings in X-linked retinoschisis. *Arch Ophthalmol.* 2007;125:259–267.

71. Millodot M. Foveal and extra-foveal acuity with and without stabilized retinal images. *Br J Physiol Opt.* 1966;23:75–106.

72. Wabbels B, Demmler A, Paunescu K, Wegscheider E, Preising MN, Lorenz B. Fundus autofluorescence in children and teenagers with hereditary retinal diseases. *Graefes Arch Clin Exp Ophthalmol.* 2006;244:36–45.

73. Robson AG, Michaelides M, Luong VA, et al. Functional correlates of fundus autofluorescence abnormalities in patients with RPGR or RIMS1 mutations causing cone or cone rod dystrophy. *Br J Ophthalmol.* 2008;92:95–102.

74. Kabanarou SA, Holder GE, Bird AC, et al. Isolated foveal retinoschisis as a cause of visual loss in young females. *Br J Ophthalmol.* 2003;87:801–803.

75. Weber BH, Schrewe H, Molday LL, et al. Inactivation of the murine X-linked juvenile retinoschisis gene, Rs1h, suggests a role of retinoschisin in retinal cell layer organization and synaptic structure. *Proc Natl Acad Sci U S A.* 2002;99:6222–6227.

76. Hendrickson AE. Primate foveal development: a microcosm of current questions in neurobiology. *Invest Ophthalmol Vis Sci.* 1994;35:3129–3133.

77. Provis JM, Hendrickson AE. The foveal avascular region of developing human retina. *Arch Ophthalmol.* 2008;126:507–511.

78. Springer AD, Hendrickson AE. Development of the primate area of high acuity, 1: use of finite element analysis models to identify mechanical variables affecting pit formation. *Vis Neurosci.* 2004; 21:53–62.

79. Robinson SR. Development of the mammalian retina. In: Dreher B, Robinson SR, eds. *Neuroanatomy of the Visual Pathways and Their Development: Vision and Visual Dysfunction.* Basingstoke, UK: MacMillan; 1991:69–128.

80. Talcott KE, Ratnam K, Sundquist SM, et al. Longitudinal study of cone photoreceptors during retinal degeneration and in response to ciliary neurotrophic factor treatment. *Invest Ophthalmol Vis Sci.* 2011;52:2219–2226.

81. Antcliff RJ, Marshall J. The pathogenesis of edema in diabetic maculopathy. *Semin Ophthalmol.* 1999;14:223–232.

82. Gass JD, Anderson DR, Davis EB. A clinical, fluorescein angiographic, and electron microscopic correlation of cystoid macular edema. *Am J Ophthalmol.* 1985;100:82–86.

83. Wolter JR. The histopathology of cystoid macular edema. *Albrecht Von Graefes Arch Klin Exp Ophthalmol.* 1981;216:85–101.

84. Bringmann A, Reichenbach A, Wiedemann P. Pathomechanisms of cystoid macular edema. *Ophthalmic Res.* 2004;36:241–249.

85. Apushkin MA, Fishman GA. Use of dorzolamide for patients with X-linked retinoschisis. *Retina.* 2006;26:741–745.

86. Ghajarnia M, Gorin MB. Acetazolamide in the treatment of X-linked retinoschisis maculopathy. *Arch Ophthalmol.* 2007;125:571–573.

87. Genead MA, Fishman GA, Walia S. Efficacy of sustained topical dorzolamide therapy for cystic macular lesions in patients with X-linked retinoschisis. *Arch Ophthalmol.* 2010;128:190–197.

88. Walia S, Fishman GA, Molday RS, et al. Relation of response to treatment with dorzolamide in X-linked retinoschisis to the mechanism of functional loss in retinoschisin. *Am J Ophthalmol.* 2009; 147:111–115, e111.

89. Takada Y, Vijayasarathy C, Zeng Y, Kjellstrom S, Bush RA, Sieving PA. Synaptic pathology in retinoschisis knockout (Rs1-/y) mouse retina and modification by rAAV-Rs1 gene delivery. *Invest Ophthalmol Vis Sci.* 2008;49:3677–3686.

90. Kjellstrom S, Bush RA, Zeng Y, Takada Y, Sieving PA. Retinoschisin gene therapy and natural history in the Rs1h-KO mouse: long-term rescue from retinal degeneration. *Invest Ophthalmol Vis Sci.* 2007; 48:3837–3845.

91. Zeng Y, Takada Y, Kjellstrom S, et al. RS-1 gene delivery to an adult Rs1h knockout mouse model restores ERG b-wave with reversal of the electronegative waveform of X-linked retinoschisis. *Invest Ophthalmol Vis Sci.* 2004;45:3279–3285.

92. Min SH, Molday LL, Seeliger MW, et al. Prolonged recovery of retinal structure/function after gene therapy in an Rs1h-deficient mouse model of X-linked juvenile retinoschisis. *Mol Ther.* 2005; 12:644–651.

93. Dyka FM, Molday RS. Coexpression and interaction of wild-type and missense RS1 mutants associated with X-linked retinoschisis: its relevance to gene therapy. *Invest Ophthalmol Vis Sci.* 2007; 48:2491–2497.